Experimental study of incomplete fusion reactions in the ^{16}O + ^{130}Te system below 6 MeV/nucleon

Devendra P. Singh,[1,*] Vijay R. Sharma,[1] Abhishek Yadav,[1] Pushpendra P. Singh,[2] Unnati,[1] M. K. Sharma,[3] R. Kumar,[4] B. P. Singh,[1,†] and R. Prasad[1]

[1]*Department of Physics, Aligarh Muslim University, Aligarh 202 002, India*

[2]*Department of Physics, Indian Institute of Technology Ropar, Rupnagar, Punjab-140001, India*

[3]*Department of Physics, S. V. College, Aligarh 202 001, India*

[4]*Inter-University Accelerator Centre, Aruna Asaf Ali Marg, New Delhi 110 067, India*

(Received 12 July 2013; revised manuscript received 25 December 2013; published 21 February 2014)

Background: The measurement and analysis of excitation functions may be used as an important tool to understand incomplete fusion reaction dynamics.

Purpose: Several studies have been carried out to study incomplete fusion reactions at low energies, but a clear picture of incomplete fusion reaction processes at energies below 6 MeV/nucleon has yet to emerge. Further, there is no theoretical model which may give a good representation of incomplete fusion processes.

Method: Off-line γ-ray spectrometry has been used to measure the excitation functions in the ^{16}O + ^{130}Te system at energies ≈3–6 MeV/nucleon.

Results: Excitation functions for five reaction products populated via complete and/or incomplete fusion processes in the ^{16}O + ^{130}Te system have been measured. Measured cross-sections have been compared with the predictions of the statistical model code PACE4. A significant enhancement in the measured excitation functions compared to theoretical predictions for α-emitting channels has been observed and is attributed to incomplete fusion processes. The relative strength of incomplete fusion has been found to increase with projectile energy. In the case of the ^{133}Xe($3\alpha n$) channel, the isomeric cross-section ratios have been deduced and found to increase rapidly with beam energy, indicating the importance of imparted angular momentum. The angular momentum at different energies has also been calculated. The analysis of the data indicates that incomplete fusion is associated even for angular momentum values smaller than the critical angular momentum for complete fusion. The results have been discussed in terms of the α-cluster structure of the projectile for various fusion reactions.

Conclusions: It may be concluded that, apart from complete fusion, incomplete fusion processes are of greater importance even at energies as low as ≈3-6 MeV/nucleon, where fusion evaporation channels are expected to be dominant. The measured isomeric cross-section ratio for the dominant incomplete fusion channel is found to increase with energy. Analysis of the data indicates that the incomplete fusion contribution becomes significant even for values of imparted angular momentum $\ell < \ell_{\text{critical}}$ also, contrary to SUMRULE model predictions.

DOI: 10.1103/PhysRevC.89.024612 PACS number(s): 25.60.Dz, 25.70.Gh, 25.70.Jj, 25.70.Mn

I. INTRODUCTION

In recent years, the investigation of incomplete fusion (ICF) processes in heavy-ion interactions around the Coulomb barrier has been a topic of interest for exploring the nuclear structure and reaction dynamics [1–9]. During such heavy-ion interactions, if the incident energy of the projectile in the center-of-mass frame is sufficient to overcome the Coulomb barrier, then the incident ion fuses with the target nucleus, leading to the formation of a composite system which may reach statistical equilibrium before decaying to various channels. Such complete fusion events may be explained with statistical model calculations. Further, as the projectile comes near the field of the target nucleus, it may break up and one of the fragments may fuse, leading to what is referred to as incomplete fusion. Cross-section measurements of different reaction channels for both the weakly as well as strongly bound projectiles with targets of medium and heavy-mass nuclei have been carried out to study the dynamics of such reaction processes [10–13]. The residues produced via complete and incomplete fusion processes have entirely different populations of angular momentum states. In heavy-ion interactions, incomplete fusion has been found to be one of the dominant modes of reaction at energies as low as ≈3–6 MeV/nucleon along with complete fusion [14,15]. In the ICF process, direct α particles have been observed in the forward cone with nearly the same velocity as that of the incident ion [16]. It may be pointed out that, at these low energies, complete fusion is supposed to be the sole contributor to the total fusion cross section [17,18]. In order to have a better understanding of incomplete fusion reaction dynamics, a program of measurement of cross-sections of populated radioactive reaction products in heavy-ion induced reactions has been undertaken by our group [14,15,19–24]. The analysis of experimentally measured excitation functions within the framework of a statistical model code may be used to obtain information about the reaction mechanisms involved [14,15,19,21]. Interestingly, α-emitting channels at energies ≈3–6 MeV/nucleon are found to show enhancement of cross-sections over the statistical model predictions, which may be due to the projectile breakup processes in these reactions, though, at higher projectile energies (⩾10 MeV/nucleon),

*dpsingh19@gmail.com

†bpsinghamu@gmail.com

Wilczynski *et al.* [25] have well explained the cross-sections for incomplete fusion reactions based on partial statistical equilibrium and on the idea of a generalized concept of angular momentum. However, on the basis of the above prescription, incomplete fusion reactions could not be explained at lower projectile energies, where the maximum angular momentum values (ℓ_{max}) are less than the critical angular momentum ($\ell_{critical}$), in general, thereby precluding any window for incomplete fusion above $\ell_{critical}$. Theoretically, the breakup of the projectile may also be understood on the basis of the disappearance of the fusion pocket in the one-dimensional effective potential energy curve, as the angular momentum (ℓ) increases beyond the critical limit ($\ell_{critical}$) for complete fusion. In order to provide sustainable input angular momentum and/or to restore the so-called pocket in the potential energy curve, the projectile may break up into clusters, one of which may fuse with the target nucleus, while the remnant escapes and carries away the excess angular momentum. Thus, there is a deficit in all nucleonic degrees of freedom of the incompletely fused composite system, compared to the composite system formed via complete fusion [14,19–22,26]. The γ-multiplicity measurements by Wilczynski *et al.* [25], Inamura *et al.* [27], Gerschel *et al.* [28], and Trautmann *et al.* [29] also indicate that such breakup fusion, in general, involves $\ell \geqslant \ell_{critical}$. However, studies [30] on spherical targets showed involvement of ℓ values in incomplete fusion lower than $\ell_{critical}$ [23] as well, giving rise to conflicting reports on the dependence of incomplete fusion on the angular momentum.

Several dynamical models [25,31–38] are proposed to explain the ICF reaction dynamics. Apart from the aforementioned dynamical models, Morgenstern *et al.* [39,40] investigated the mass-asymmetry dependence of breakup fusion. In one of our recent communications [15] the α Q value of the projectile has been found to play an important role in incomplete fusion processes. It may be pointed out that the available theoretical models [25,31–38] satisfactorily predict the magnitude of incomplete fusion contribution, to some extent, in some cases at energies $\geqslant$10 MeV/nucleon, but none of these models is able to successfully explain such data at low energies. In view of the above, a clear picture of the mechanism of incomplete fusion has yet to emerge, particularly at relatively low bombarding energies, i.e., ≈3–5 MeV/nucleon, where systematic studies are scarce [20,21], and needs to be explored in a systematic way. The present measurements are part of a series of incomplete fusion studies, in which excitation functions and recoil range distributions have been measured to obtain the systematics for ICF reactions at low energies. In the present work, the cross-sections for five reaction products populated in the interaction of $^{16}O + ^{130}Te$ have been measured in a broad projectile energy range of ≈60–90 MeV.

II. EXPERIMENT

A beam of $^{16}O^{7+}$ obtained from the 15-UD Pelletron accelerator of the Inter-University Accelerator Center, New Delhi, India, has been used to carry out the experiments. The ^{130}Te target samples (enrichment ≈61%) were prepared by vacuum evaporation on Al foils of thickness ≈6.75 mg/cm^2. The Al backing served as an energy degrader as well as a catcher foil to trap the energetic recoiling residues. The thickness of sample deposition in each target was determined by the α-transmission method, which is based on the measurement of the energy lost by 5.487-MeV α particles, obtained from a standard ^{241}Am source, while passing through the target material. The measured thicknesses of the ^{130}Te deposition in different samples were ≈1.8 mg/cm^2. Two stacks containing two ^{130}Te samples each, followed by Al catchers, were irradiated at 85 and 90 MeV, respectively, in the General Purpose Scattering Chamber. Proper care has been taken to maintain a constant beam current (≈3 pnA) throughout the irradiations. The beam flux was calculated from the total charge collected in a Faraday cup, placed behind the target-catcher stack foil assembly. Both irradiations were carried out for ≈8 h duration. After the irradiation, by using an in-vacuum transfer facility the sample along with the catcher was taken to a high-purity Ge detector for γ counting. The γ-ray activities of the residues were measured using ORTEC's 100 cc active volume high-purity Ge detector coupled to a personal-computer-based 8 000-channel multichannel analyzer employing FREEDOM software [41]. The resolution of the detector system was ≈2 keV full width at half maxima for the 1332.0-keV γ line of ^{60}Co. The dead time of the detector system was always kept less than 10%. The γ-ray counting of the sample was done several times with increasing counting time to follow the decay and to have good statistics for the photopeaks of the γ lines of different residues. As a representative case, a typical γ-ray spectrum of the residues from a sample irradiated by an ≈90 MeV oxygen beam is shown in Fig. 1, where various peaks corresponding to reaction residues populated via different reaction channels are indicated. The reaction residues of interest have been identified by their measured half-lives ($T_{1/2}$) and characteristic γ-ray energies. Identified reaction products along with some of their important spectroscopic properties are given in Table I. The measured intensities of the characteristic γ lines of the identified residues have been used to calculate the cross-sections for the corresponding reaction

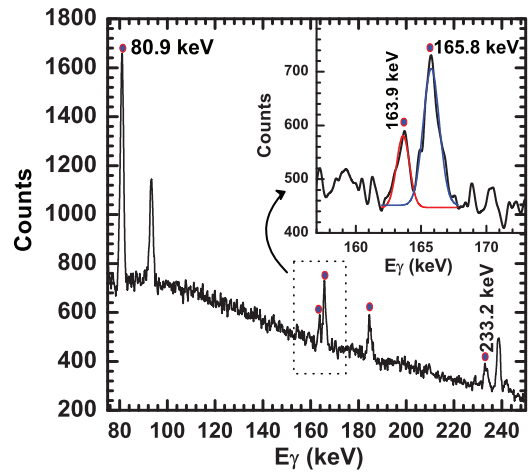

FIG. 1. (Color online) Observed γ-ray spectrum of a ^{130}Te sample irradiated by an ≈90 MeV $^{16}O^{7+}$ beam.

TABLE I. List of identified reaction products along with respective channels and their spectroscopic properties.

Residue (channels)	$T_{1/2}$	J^{π}	E_{γ} (keV)	I_{γ} (%)
^{141}Nd$^{g}(5n)$	2.49 h	$3/2^{+}$	1127	0.8
^{139}Ce$^{g}(\alpha 3n)$	137.6 d	$3/2^{+}$	165.8	79.9
^{133}Xe$^{m}(3\alpha n)$	2.19 d	$11/2^{-}$	233.2	10.3
^{133}Xe$^{g}(3\alpha n)$	5.2 d	$3/2^{+}$	80.9	73
^{131}Xe$^{m}(3\alpha 3n)$	11.9 d	$11/2^{-}$	163.9	1.97

channels, by employing a FORTRAN program based on standard formulations [21]. A critical evaluation of the uncertainties in the measured cross-sections has been considered. The errors in the measured cross-sections may arise due to (a) nonuniform deposition of the target material and inaccurate estimate of the foil thickness, which may be $\leqslant$1%, (b) fluctuations in the beam current during the irradiations, which may result in the variation of the incident flux. Many tests were performed to check the time-integrated beam fluctuations and it was estimated that beam fluctuations may introduce errors of not more than 5% in the measured cross-sections. Errors in the production cross-sections may also result from (c) uncertainty in the determination of the geometry-dependent efficiency of the γ-ray spectrometer. Further, uncertainty in determining the efficiency of the spectrometer may also appear due to the solid-angle effect, as the irradiated samples were not point sources like the standard source but had a finite diameter, which may be $\leqslant$5%. Large errors in the measured cross-sections may also be introduced by (d) the product nuclei recoiling out of the thin target. In the present measurements the targets were oriented perpendicular to the beam direction with the sample deposition facing the beam. This avoids the loss of recoiling nuclei which were stopped in the relatively thick ($\approx$6.75 mg/cm^2) aluminum backing and were counted along with the sample. In this way, the loss due to recoil was eliminated. Further, the uncertainties in the nuclear data, such as branching ratio, decay constant, etc., which have been taken from the Table of Isotopes [42], have not been taken into consideration. Details of above-mentioned factors that may introduce uncertainties are given in Ref. [21]. The overall error in the measured data is estimated to be $\leqslant$15%, including that due to statistical errors.

III. ANALYSIS AND INTERPRETATION OF RESULTS

The cross-sections for the reactions ^{130}Te(^{16}O,5n)^{141}Nd, ^{130}Te(^{16}O,$\alpha 3n$)^{139}Ce, ^{130}Te(^{16}O,3αn)^{133}Xe^{m}, ^{130}Te(^{16}O,3αn)^{133}Xe^{g}, and ^{130}Te(^{16}O,3α3n)^{131}Xe^{m} have been measured in the energy range of $\approx$60–90 MeV and are tabulated in Table II. It may be pointed out that, out of the possible complete fusion channels, only 5n channel residues [^{141}Nd ($t_{1/2}$ = 2.49 h)] could be identified. The other fusion evaporation residues [^{145}Nd (through one-neutron emission)] are stable (8.3%), the residues populated via the 2n channel (^{144}Nd) are stable (23.8%), ^{143}Nd residues populated via the 3n channel are stable (12.2%), and ^{142}Nd residues populated through 4n emission are also stable (27.2%). Hence, these residues could not be identified in the present work. In the present case, the ^{141}Nd residues may be formed by the fusion of ^{16}O + ^{130}Te, forming the composite system ^{146}Nd* followed by the evaporation of five neutrons. The ^{141}Nd^{g} residues have been identified by the characteristic γ-ray of an energy of 1127 keV and also by measuring its half-life using decay curve analysis. Further, the ^{139}Ce residues may be formed by the complete fusion of ^{16}O and ^{130}Te, forming the composite system ^{146}Nd*, which may decay by the evaporation of an α particle and three neutrons. The same ^{139}Ce residues may also be produced if the fragment ^{12}C (if ^{16}O undergoes breakup into an α particle and ^{12}C fragments) fuses with the ^{130}Te target nucleus followed by the evaporation of three neutrons. As a representative case, the modes of formation of ^{139}Ce residues which may be populated via both complete fusion and/or incomplete fusion reaction channels are as follows:

(a) population of ^{139}Ce via complete fusion of ^{16}O:

$$^{16}\mathrm{O} + {}^{130}\mathrm{Te} \Longrightarrow {}^{146}\mathrm{Nd}^{*} \Longrightarrow {}^{139}\mathrm{Ce} + \alpha + 3n,$$

(b) population of ^{139}Ce via incomplete fusion of ^{16}O:

$$^{16}\mathrm{O}(^{12}\mathrm{C} + \alpha) + {}^{130}\mathrm{Te} \Longrightarrow {}^{142}\mathrm{Ce}^{*} + \alpha(\text{spectator}),$$
$$^{142}\mathrm{Ce}^{*} \Longrightarrow {}^{139}\mathrm{Ce} + 3n.$$

In the same way, ^{133}Xe^{g,m} and ^{131}Xe^{m} residues may also be formed by complete fusion as well as incomplete fusion processes.

Theoretical calculations of cross-sections for the residues populated via complete fusion channels have also been done using the code PACE4 [43] (an upgraded version of the theoretical model code PACE2 [44]), which is based on Hausher-Feshbach formalism followed by Monte Carlo simulation to determine the decay sequence of an excited compound nucleus. Bass formulations [45] are used to calculate the cross-sections for a particular reaction channel. For compound nucleus formation, at a particular angular momentum ℓ and specific bombarding energy E, the partial cross section σ_{ℓ} is

TABLE II. Experimentally measured cross-sections for the residues populated in the interaction of the ^{16}O + ^{130}Te system.

Laboratory energy (MeV)	σ(^{141}Nd) (mb)	σ(^{139}Ce) (mb)	σ(^{133}Xe^{m}) (mb)	σ(^{133}Xe^{g}) (mb)	σ(^{131}Xe^{m}) (mb)
61.3 ± 2.2	2.2 ± 0.2	–	8 ± 2	5.1 ± 0.8	8 ± 1
67.1 ± 2.1	20 ± 2	107 ± 11	183 ± 30	30 ± 3	12 ± 2
83.2 ± 1.8	682 ± 84	89 ± 8	180 ± 25	34 ± 3	180 ± 20
90.1 ± 1.9	685 ± 85	183 ± 18	477 ± 60	80 ± 10	320 ± 40

given by

$$\sigma_\ell = \frac{\lambda^2}{4\pi}(2\ell+1)T_\ell, \tag{1}$$

where λ is the reduced wavelength and the transmission coefficients T_ℓ may be given by the expression

$$T_\ell = \left[1+\exp\left(\frac{\ell-\ell_{\max}}{\Delta}\right)\right]^{-1}, \tag{2}$$

where Δ is the diffuseness parameter, while $\ell_{\max}$ is the maximum value of ℓ determined by total fusion cross section

$$\sigma_F = \sum_{\ell=0}^{\infty}\sigma_\ell. \tag{3}$$

The projections of angular momentum are calculated at each stage of de-excitation. The default optical model parameters for neutrons, protons, and α particles are used [46]. The γ-ray strength functions for $E1$, $E2$, and $M1$ transitions are taken from the tables of Endt [47]. The code has been modified to take into account the excitation energy dependence of the level density parameter using the prescription of Kataria *et al.* [48]. The detailed discussion of this code is given in one of our recent works [21]. However, for the sake of completeness, it may be mentioned that nuclear level density, i.e., the number of levels per unit energy at a particular excitation energy, is an important parameter in any statistical analysis of nuclear reactions. In this code, the level density parameter $a(=A/K)$ mainly governs the equilibrium state. Here, A is the atomic mass number of the compound nucleus and K is a free parameter, which may be varied to match the experimental data. A value of $K=10$ has been suggested [14] to be a physically reasonable value and explains the data satisfactorily. Therefore, in the present work, the value of $K=10$ has been retained and the calculations have been carried out by keeping the values of fusion radius, yrast spin, maximum angular momenta, ℓ diffuseness, etc. as default values. It may, however, be pointed out that a value of $K>10$ may give rise to the anomalous effect in particle multiplicity and compound nucleus temperature [49]. It may be mentioned here that in this code the ICF of the incident ion is not taken into consideration, so any enhancement in the measured cross section compared to PACE4 code predictions may be attributed to breakup fusion channels.

In Fig. 2, the measured cross-sections, i.e., $\sigma_{\text{expt}}(5n)$, for the ^{130}Te(^{16}O,$5n$)^{141}Nd reaction have been compared with the theoretical predictions of the statistical model code PACE4 [43]. As can be seen from this figure, the experimentally measured cross-sections for the ^{141}Nd residues populated via the $5n$ channel are found to be nicely reproduced by statistical model predictions, which indicates its production through the complete fusion process only. In the present case, the isomeric state of ^{141}Nd ($t_{1/2}\approx 61$ s) decays completely via isomeric transition (IT) to the ground state of ^{141}Nd. Consequently, the measured activity of ^{141}Nd^g (identified by $E_\gamma = 1127$ keV and $t_{1/2}\approx 2.49$ d) may be considered as the total sum of metastable and ground states of ^{141}Nd. It may be pointed out that several xn and pxn channels in the studied energy range

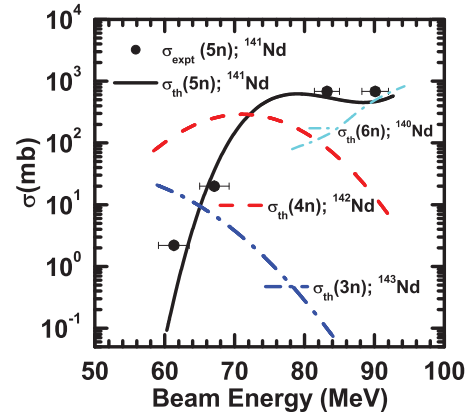

FIG. 2. (Color online) Measured excitation functions for ^{141}Nd($5n$) isotopes. Lines indicate the theoretical calculations for the residues ^{140,141,142,143}Nd.

could not be measured due to their stable nature and/or very low γ-ray intensities of corresponding residues. Therefore, the excitation functions for dominant reaction channels (i.e., $3n$, $4n$, and $6n$), which could not be measured, were also calculated by using consistently the same set of parameters and these are also shown in Fig. 2. The α-emitting channels need special mention. The $\alpha 3n$ channel gives rise to the population of ^{139}Ce. The isomeric state of ^{139}Ce ($t_{1/2}\approx 56$ s) decays completely via IT to the ground state of ^{139}Ce. Therefore, the measured activity of ^{139}Ce^g may be taken as the sum of the metastable and ground states of ^{139}Ce. In Fig. 3, excitation functions for the reaction products populated in

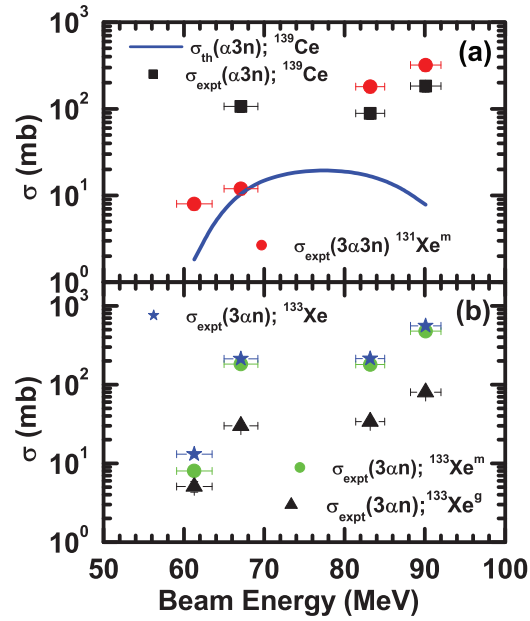

FIG. 3. (Color online) (a) Experimentally measured and theoretically calculated ($K=10$) excitation functions for ^{139}Ce($\alpha 3n$) and ^{131}Xe^m($3\alpha 3n$) channels and (b) experimentally measured cross-sections for ^{133}Xe^m($3\alpha n$) and ^{133}Xe^g($3\alpha n$) channels along with the total cross-sections for ^{133}Xe.

α-emitting channels (expected to be populated via complete and/or incomplete fusion) are presented. Figure 3(a) shows a comparison of measured cross-sections for the production of ^{139}Ce and ^{131}Xe^{m} residues populated via α3n and 3α3n channels, respectively, with the theoretical predictions of the code PACE4. It may be seen from Fig. 3(a) that the measured values of the cross-sections for the ^{139}Ce(α3n) residues underestimate the theoretical predictions by an order of magnitude, while PACE4 gives a negligible cross section for the ^{131}Xe(3α3n) residues, indicating that these residues are populated predominantly via breakup fusion processes. The measured reaction residues may have a contribution from their higher charge isobar precursor as well. In case of the α3n channel, the ^{139}Ce residues may also have a contribution from its higher charge isobar precursor ^{139}Pr (formed via the $p6n$ channel) decaying by β^{-} emission. It may be pointed out that the theoretical calculations done with PACE4 give negligible contribution for the population of ^{139}Pr via the $p6n$ channel. Thus, there is less likelihood of ^{139}Pr decay via β^{-} emission feeding the population of ^{139}Ce. Similarly, in case of the 3αn channel populating ^{133}Xe residues, the precursor ^{133}Cs is found to be stable and hence no contribution to ^{133}Xe from precursor decay is expected. However, in case of ^{131}Xe^{m} (11.9 d) populated via the 3α3n channel, the contribution of precursor ^{131}Cs (9.9 d) could not be estimated in the absence of intense γ lines of the precursor residue. As such, the cross section for the ^{131}Xe^{m}(3α3n) population may be considered as a cumulative sum of 3α3n and 2$\alpha p6n$ channels. In view of the above description, it may be noted that the β activity does not affect the finally obtained results, in general. In Fig. 3(b), the measured cross-sections for the production of both the isomeric and ground states of ^{133}Xe (3αn) isotopes are shown. The measured cross-sections for these residues produced via α-emitting channels could not be compared with the predictions of the code PACE4, as it gives negligible probability for this channel. As such, the 3α3n channel is likely to have a dominant mode of population via an incomplete fusion or a breakup fusion channel. In order to determine the ICF contribution to the measured α-emitting channels, the measured $\Sigma\sigma^{\alpha}_{\rm expt}$ (sum of cross-sections of all measured α-emitting channels) has been compared with the corresponding calculated values based on complete fusion calculations, i.e., $\Sigma\sigma^{\alpha}_{Th}$. Since PACE4 does not take incomplete fusion into consideration, the calculated cross-sections for α3n, 3αn, and 3α3n channels will have predictions based on the complete fusion model only. In Fig. 4(a), a comparison of $\Sigma\sigma^{\alpha}_{\rm expt}$ has been made with corresponding $\Sigma\sigma^{\alpha}_{Th}$ calculated using PACE4. It may be observed from Fig. 4(a) that the $\Sigma\sigma^{\alpha}_{Th}$ obtained from PACE4 predictions significantly underestimates the $\Sigma\sigma^{\alpha}_{\rm expt}$ in the entire energy range. The enhancement of the experimental values compared to the theoretical predictions may be due to the incomplete fusion processes and has been denoted by $\sigma_{\rm ICF}$. It may also be noted that the difference between $\Sigma\sigma^{\alpha}_{\rm expt}$ and $\Sigma\sigma^{\alpha}_{Th}$ increases with energy throughout the entire energy region of interest, indicating the dominance of incomplete fusion with a maximum ICF contribution at the highest studied energy. In Fig. 4(a), the ratio of $\Sigma\sigma^{\alpha}_{\rm expt}$ to $\Sigma\sigma^{\alpha}_{Th}$ has been plotted to show the importance of incomplete fusion processes as the energy increases.

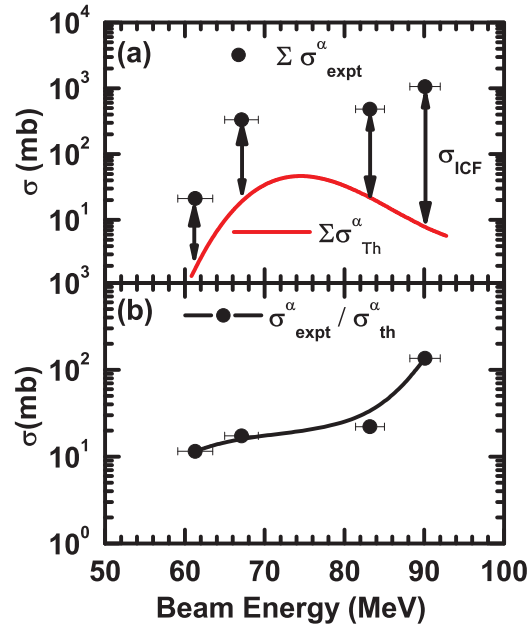

FIG. 4. (Color online) Comparison of the sum of the measured cross-sections for α-emitting channels i.e., $\Sigma\sigma^{\alpha}_{\rm expt}$, and calculated values $\Sigma\sigma^{\alpha}_{Th}$. The increasing difference between the experimental and calculated values with energy indicates the dominance of incomplete fusion processes with energy. Lines joining the data points in (b) are just to guide the eyes.

The isomeric cross-section ratios (ICRs) for the residues populated in the reaction ^{130}Te(^{16}O,3αn)^{133}Xe produced via complete and/or incomplete fusion channels are shown in Fig. 5. It may be seen from this figure that the ICR increases with energy, in general. Since the ICF reactions are considered to take place in peripheral collisions, a relatively large amount of angular momentum is transferred, and this may increase with energy. The increase in isomeric population with energy indicates that a part of the input angular momentum may get converted to the nuclear spin and the isomeric population may increase. Thus, the ICR may depend strongly on the relative

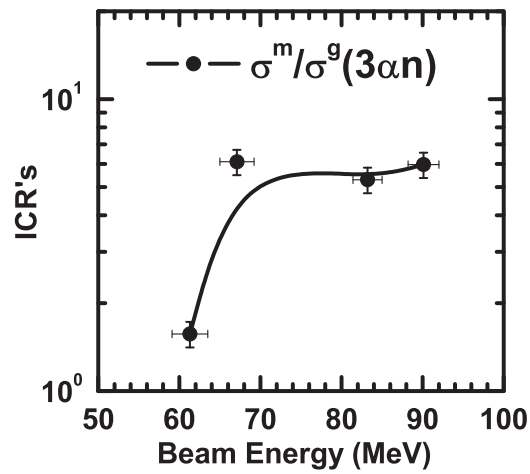

FIG. 5. Isomeric cross-section ratios for the residues ^{133}Xe(3αn). The line drawn is just to guide the eyes.

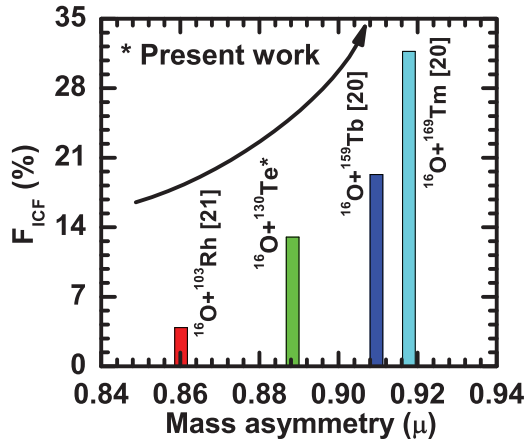

FIG. 6. (Color online) The percentage incomplete fusion fraction ($F_{\rm ICF}$) as a function of mass asymmetry at a constant relative velocity ($\beta = 0.055c$) for the presently studied system along with results from the literature [20,21].

spins of metastable and ground states and also on the energy difference between the levels. Further, an attempt has also been made to investigate the mass-asymmetry systematics. In order to study the dependence of incomplete fusion on the mass asymmetry of interacting partners, the percentage incomplete fusion fraction (%$F_{\rm ICF}$) has been deduced for the presently studied system. $F_{\rm ICF}$ is a measure of the relative strength of incomplete fusion to that of total fusion defined as $F_{\rm ICF}(\%) = (\Sigma\sigma_{\rm ICF}/\sigma_{\rm ICF}) \times 100$. Morgenstern *et al.* [39,40], suggest that the onset of incomplete fusion is governed by the relative velocity of the projectile (β) and mass asymmetry [$\mu = A_T/(A_T + A_P)$] of the interacting partner and starts contributing significantly above $\beta \approx 0.06c$ (i.e., 6% of c, where c is the speed of light). In order to understand how the incomplete fusion fraction varies with the entrance channel mass asymmetry (μ), the value of $F_{\rm ICF}(\%)$ for the ^{16}O + ^{130}Te system has been compared with those found in the literature [20,21] at a constant relative velocity ($\beta = 0.055c$). Figure 6 shows the incomplete fusion strength as a function of μ. $F_{\rm ICF}$ is found to increase with mass asymmetry (μ) for the ^{16}O projectile with different targets. As inferred from this figure, the incomplete fusion probability is higher for more mass-asymmetric systems, which is in accordance with the Morgenstern mass-asymmetry systematics developed for energies $\geqslant$10 MeV/A, in general. We propose to measure the contribution of the presently studied α-emission channels in an in-beam experiment using a particle-γ coincidence technique, so that the present data may be supplemented.

Further, it is possible to calculate the cross-sections for complete and incomplete fusion channels separately using the SUMRULE model [50,51], based on the idea of a generalized concept of critical angular momentum following partial statistical equilibrium. The underlying assumption in the SUMRULE model is that the ICF channels open up only for those partial waves which have ℓ values greater than $\ell_{\rm critical}$ (i.e., $\ell \geqslant \ell_{\rm critical}$). On the other hand, partial waves with $\ell < \ell_{\rm critical}$ contribute to complete fusion. The limiting angular momentum of the entrance channel, $\ell_{\rm limit}$, is related to the critical angular momentum $\ell_{\rm crit}^{P^p+T}$ of the fused part as

$$\ell_{\rm limit} = \frac{A_p \cdot A_T}{(A_{P^s} \cdot A_p + A_{P^p} \cdot A_T)} \cdot \ell_{\rm crit}^{P^p+T}, \tag{4}$$

where P^p represents the participant and P^s the spectator. However, for a mass-asymmetric projectile-target combination, the limiting angular momentum may be rewritten as

$$\ell_{\rm limit} \sim \frac{A_p}{A_{P^p}} \cdot \ell_{\rm crit}^{P^p+T}. \tag{5}$$

The transmission coefficients T_ℓ(i) for individual reaction channels, obtained by assuming a smooth cutoff in ℓ space, is given as

$$T_\ell(i) = \left[1 + \exp\left(\frac{\ell - \ell_{\rm limit}(i)}{\Delta}\right)\right]^{-1}, \tag{6}$$

where Δ is the diffuseness in the ℓ distribution. For relatively lower ℓ values, the transmission coefficients are almost unity for all the channels. The different reaction channels are considered to open up one after the other with increasing angular momentum and depending on their corresponding limiting angular momenta $\ell_{\rm limit}(i)$. Hence, the reaction probabilities for a given partial wave ℓ are

$$N_\ell \sum_i T_\ell(i) \exp\left[\frac{Q_{gg}(i) - Q_c(i)}{T}\right] = 1, \tag{7}$$

where N_ℓ is the ℓ-dependent normalization factor common for all reaction channels, Q_{gg} [=log($d\sigma/d\Omega$)] [25,50,51], is the ground state Q value, Q_c is the change in the Coulomb interaction energy due to the transfer of charge, and T is an effective temperature. Thus, the absolute cross section for the individual reaction channels is defined as

$$\sigma(i) = \pi\bar{\lambda}^2 \sum_{\ell=0}^{\ell_{\rm max}} (2\ell+1) \frac{T_l(i) \cdot p(i)}{\sum_j T_l(j) \cdot p(j)}, \tag{8}$$

where $\bar{\lambda} = \hbar/\sqrt{(2\mu E)}$ is the reduced wavelength for the entrance channel and $p(i)$ is the reaction probability for a given channel i, which is proportional to $\exp\{[Q_{gg}(i) - Q_c(i)]/T\}$. $\ell_{\rm max}$ is defined as the largest ℓ for which the colliding system penetrates into the region where the total nucleus-nucleus potential is attractive and/or the distance of closest approach is smaller than the sum of the half-density radii; however, the critical angular momenta $\ell_{\rm critical}$, which determines the magnitude of the transmission coefficients T_ℓ for individual reaction channels, were calculated from a simplified formula as

$$\ell_{\rm crit}^2 = \frac{\mu_m (C_1 + C_2)^3}{\hbar^2} \left[4\pi\gamma \frac{C_1 C_2}{C_1 + C_2} - \frac{Z_1 Z_2 e^2}{(C_1 + C_2)^2}\right], \tag{9}$$

where μ_m is the reduced mass of the interacting partners, γ is the surface tension coefficient, and Z_1 and Z_2 and C_1 and C_2 are the atomic numbers and half-density radii of the projectile and the target nuclei, respectively. There are three important parameters in the model, i.e., the effective temperature T of the contact zone, the diffuseness Δ of the T_ℓ distribution, and the effective Coulomb interaction radius R_c. The values $T = 3.5$ MeV, $\Delta = 1.7\hbar$, and $R_c/(A_P^{1/3} + A_T^{1/3}) = 1.5$ fm have been suggested [50] for these parameters. The

TABLE III. Theoretically calculated cross-sections obtained by using the SUMRULE model for the residues populated via $\alpha 3n$ and $3\alpha xn$ ($x = 1, 3$) channels in the interaction of the $^{16}O + ^{130}Te$ system.

Energy (MeV)	$\sigma(^{139}Ce)$ $(\alpha 3n)$ (mb)	$\sigma(^{133}Xe^{m})$ $(3\alpha n)$ (mb)	$\sigma(^{133}Xe^{g})$ $(3\alpha n)$ (mb)	$\sigma(^{131}Xe^{m})$ $(3\alpha 3n)$ (mb)
61.3 ± 2.2	0.00811	0.00087	0.00093	0.00001
67.1 ± 2.1	0.0255	0.00275	0.00294	0.00003
83.2 ± 1.8	0.0718	0.00812	0.00868	0.00008
90.1 ± 1.9	0.115	0.0602	0.0644	0.00023

cross-sections calculated by using the SUMRULE model for the presently measured incomplete fusion channels, populated in the system $^{16}O + ^{130}Te$ at ≈61, 67, 83, and 90 MeV incident energies, are given in Table III. It has been observed that there is a large discrepancy between the measured (Table II) and SUMRULE-calculated cross-sections (Table III) for the α-emitting channels. It may be pointed out that Siwek-Wilczynska *et al.* [51] tested the SUMRULE calculations for reactions at $\geqslant$10 MeV/nucleon energies. The calculations, carried out for the presently studied system, which allow incomplete fusion processes only for $\ell > \ell_{\text{critical}}$, underestimate the measured incomplete fusion cross-section data by a few orders of magnitude. As a typical example, the experimentally measured cross section for the $\alpha 3n$ channel is 183 ± 18 mb at ≈90 MeV; however, the prediction from the SUMRULE model is only ≈0.12 mb. These discrepancies may indicate a need to refine the basic assumptions of the model for low energies. Similar deviations have also been found by Parker *et al.* [52], in their study on the $^{12}C + ^{51}V$ system up to 100 MeV (≈8 MeV/nucleon). The model assumes sharp cutoff ℓ values for complete and incomplete fusion processes. One of the possible reasons for the disagreement between the presently measured and SUMRULE calculations for incomplete fusion channels may be the nonvalidity of the concept of critical angular momentum at these low energies. The present findings indicate that a diffused boundary in ℓ space may penetrate close to the barrier, such that fusion may take place even for $\ell < \ell_{\text{critical}}$.

In order to ascertain the above in the ℓ distribution for the $^{16}O + ^{130}Te$ system, the ℓ_{critical} value has been calculated [25] and is found to be $53\hbar$. Figure 7 shows the fusion ℓ distributions for the $^{16}O + ^{130}Te$ system calculated using the code CCFULL [53] at two extreme energies: 61 and 90 MeV, respectively. The code CCFULL estimates the fusion ℓ distribution of the compound nucleus under the influence of couplings between the relative motion and nuclear collective motions. In coupled channel calculations, for heavy-ion reactions, one may use the iso-centrifugal approximation where angular momentum of the relative motion in each channel may be replaced by the total angular momentum [54], then the coupled channel equation may be given as

$$\left[+\frac{\hbar^2}{2\mu}\frac{d^2}{dr^2} - \frac{J(J+1)\hbar^2}{2\mu r^2} - V_N^{(0)}(r) - \frac{Z_P Z_T e^2}{r} - \epsilon_n + E\right] \times \psi_n(r) = \sum_m V_{nm}(r)\psi_m(r), \tag{10}$$

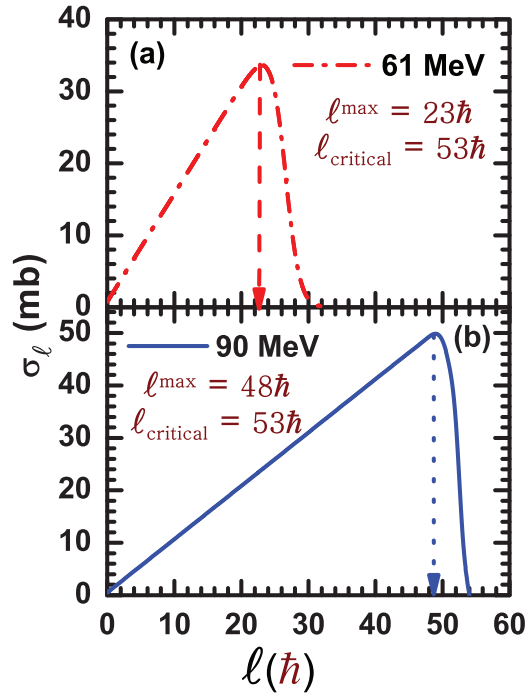

FIG. 7. (Color online) Fusion ℓ distributions calculated by using the code CCFULL for the $^{16}O + ^{130}Te$ system at $E_{\text{lab}} \approx 61$ and 90 MeV. The values of ℓ_{critical} for fusion are calculated using the formulations [25].

where μ is the reduced mass, r is the radial component of the coordinate of the relative motion, E is the projectile energy, and ϵ_n is the excitation energy of the nth channel. V_{nm} are the matrix elements of the Hamiltonian coupling including the Coulomb and nuclear components. $V_N^{(0)}$ is the nuclear potential in the entrance channel and is given by the Woods-Saxon parametrization as

$$V_N^{(0)}(r) = -\frac{V_0}{1 + \exp[(r - R_0)/a]}, \qquad R_0 = r_0\left(A_P^{1/3} + A_T^{1/3}\right). \tag{11}$$

The coupled channel calculations are done by imposing the boundary conditions, which are valid for heavy-ion reactions, that there are only incoming waves at $r = r_{\text{min}}$ and only outgoing waves at infinity for all channels except the entrance channel. The code CCFULL adopts the minimum position of the Coulomb pocket inside the barrier for r_{min}.

The fusion ℓ distributions, for the presently studied $^{16}O + ^{130}Te$ system, calculated using the CCFULL code at energies of 61 and 90 MeV, are shown in Figs. 7(a) and 7(b), respectively. The values of ℓ_{max} at two energies (61 and 90 MeV) are found to be ≈$23\hbar$ and $48\hbar$, respectively; these are less than the ℓ_{critical} value ($53\hbar$) for fusion for the present system. From Fig. 7, it may also be seen that, even at the highest studied energy, the maxima of ℓ values are not as high as ℓ_{critical} for fusion. Thus, the ICF contributions are expected to be negligible at these energies. However, the present measurements for incomplete fusion channels suggest that a significant number of partial waves below ℓ_{critical} may

contribute to incomplete fusion channels. It may be pointed out that the α particles in the incomplete fusion reactions may be emitted at forward angles with essentially the beam velocity, consistent with the breakup of the projectile close to the maximum impact parameter and therefore somewhere at the peak of the triangular fusion ℓ distribution. The above observations have been supported by our earlier studies on the measurement of the side-feeding intensity pattern, where incomplete fusion is shown to originate from a narrow-ℓ window [24].

In the present work, excitation functions for the production of the radionuclides ^{141}Nd($5n$), ^{139}Ce($\alpha 3n$), ^{133}Xe^{g}(3αn), ^{133}Xe^{m}($3\alpha n$), and ^{131}Xe^{m}($3\alpha 3n$) have been measured in the system ^{16}O + ^{130}Te in the ≈60–90 MeV energy range. The complete fusion cross-sections are found to be in agreement with PACE4 predictions over the entire energy range. However, in the case of α-emitting channels, the observed enhancement of cross-sections over the predictions of statistical model calculations obtained using the code PACE4 may be attributed to the prompt breakup of the projectile (^{16}O into ^{12}C + α and α + ^{12}C), leading to incomplete fusion processes. A comparison of data for incomplete fusion contribution for the same projectile with different targets indicates a strong and increasing trend of target mass number and mass asymmetry dependence. The SUMRULE model calculations highly underestimate the incomplete fusion cross-sections, indicating the nonvalidity of the model assumption that a substantial contribution to incomplete fusion comes from collision trajectories with $\ell > \ell_{\text{critical}}$. In the energy range of the present study, calculations indicate that ℓ_{max} is less than ℓ_{critical}; thus, significant cross-sections for incomplete fusion channels at these beam energies indicate the contribution from collision trajectories with $\ell < \ell_{\text{critical}}$ as well. The results obtained from the excitation functions give valuable information for establishing the complete and incomplete fusion yields at relatively low bombarding energies. More data on such reactions are needed to explore the above aspects, so that the assumptions of the SUMRULE model for energies near the barrier, where $\ell < \ell_{\text{critical}}$, may be improved upon to explain the experimental data.

ACKNOWLEDGMENTS

The authors are grateful to the Director of IUAC, New Delhi, India, for providing facilities to carry out the experiments. RP, BPS and VRS thank to UGC (Project No. 40-418/2011/SR) and DST (Project No. SR/S2/HEP-30/2011). DPS thanks DST for providing financial support through Project No. SR/FTP/PS-025/2011 under the Fast Track Scheme for Young Scientists.

[1] F. Michel, G. Reidemeister, and S. Ohkubo, Phys. Rev. Lett. **89**, 152701 (2002).
[2] A. Diaz-Torres and I. J. Thompson, Phys. Rev. C **65**, 024606 (2002).
[3] P. R. S. Gomes, I. Padron, E. Crema, O. A. Capurro, J. O. Fernández Niello, A. Arazi, G. V. Marti, J. Lubian, M. Trotta, A. J. Pacheco, J. E. Testoni, M. D. Rodríguez, M. E. Ortega, L. C. Chamon, R. M. Anjos, R. Veiga, M. Dasgupta, D. J. Hinde, and K. Hagino, Phys. Rev. C **73**, 064606 (2006).
[4] P. R. S. Gomes *et al.*, Phys. Lett. B **601**, 20 (2004).
[5] M. Das Gupta, D. J. Hinde, A. Mukherjee, and J. O. Newton, Nucl. Phys. A **787**, 144 (2007).
[6] S. Chakrabarty, B. S. Tomer, A. Goswami, G. K. Gubbi, S. B. Manohar, A. Sharma, B. B. Kumar, and A. Mukherjee, Nucl. Phys. A **678**, 355 (2000).
[7] D. J. Hinde, M. Dasgupta, B. R. Fulton, C. R. Morton, R. J. Wooliscroft, A. C. Berriman, and K. Hagino, Phys. Rev. Lett. **89**, 272701 (2002).
[8] K. S. Babu, R. Tripathi, K. Sudarshan, B. D. Srivastava, A. Goswami, and B. S. Tomer, J. Phys. G: Nucl. Part. Phys. **29**, 1011 (2003).
[9] A. Mukherjee *et al.*, Phys. Lett. B **636**, 91 (2006).
[10] M. Das Gupta, D. J. Hinde, R. D. Butt, R. M. Anjos, A. C. Berriman, N. Carlin, P. R. S. Gomes, C. R. Morton, J. O. Newton, A. S. Toledo, and K. Haginoa, Phys. Rev. Lett. **82**, 1395 (1999).
[11] M. Das Gupta *et al.*, Phys. Rev. C **66**, 041602(R) (2002).
[12] L. R. Gasques, D. J. Hinde, M. Das Gupta, A. Mukharjee, and P. R. S. Gomes, Phys. Rev. C **79**, 034605 (2009).
[13] M. Das Gupta *et al.*, Annu. Rev. Nucl. Part. Sci. **48**, 40161 (1998).
[14] D. P. Singh, Unnati, P. P. Singh, A. Yadav, M. K. Sharma, B. P. Singh, K. S. Golda, R. Kumar, A. K. Sinha, and R. Prasad, Phys. Rev. C **80**, 014601 (2009).
[15] A. Yadav, V. R. Sharma, P. P. Singh, R. Kumar, D. P. Singh, Unnati, M. K. Sharma, B. P. Singh, and R. Prasad, Phys. Rev. C **86**, 014603 (2012).
[16] H. C. Britt and A. R. Quinton, Phys. Rev. **124**, 877 (1961).
[17] M. Dasgupta, P. R. S. Gomes, D. J. Hinde, S. B. Moraes, R. M. Anjos, A. C. Berriman, R. D. Butt, N. Carlin, J. Lubian, C. R. Morton, J. O Newton, and A. Szanto de Toledo, Phys. Rev. C **70**, 024606 (2004).
[18] L. F. Canto, R. Donangelo, L. M. de Matos, M. S. Hussein, and P. Lotti, Phys. Rev. C **58**, 1107 (1998).
[19] D. P. Singh, Unnati, P. P. Singh, A. Yadav, M. K. Sharma, B. P. Singh, K. S. Golda, R. Kumar, A. K. Sinha, and R. Prasad, Phys. Rev. C **81**, 054607 (2010).
[20] P. P. Singh, B. P. Singh, M. K. Sharma, Unnati, D. P. Singh, R. Prasad, R. Kumar, and K. S. Golda, Phys. Rev. C **77**, 014607 (2008).
[21] Unnati, P. P. Singh, D. P. Singh, M. K. Sharma, A. Yadav, R. Kumar, B. P. Singh, and R. Prasad, Nucl. Phys. A **811**, 77 (2008).
[22] P. P. Singh, B. P. Singh, M. K. Sharma, Unnati, R. Kumar, K. S. Golda, D. Singh, R. P. Singh, S. Muralithar, M. A. Ansari, R. Prasad, and R. K. Bhowmik, Phys. Rev. C **78**, 017602 (2008).
[23] A. Yadav, V. R. Sharma, P. P. Singh, D. P. Singh, M. K. Sharma, U. Gupta, R. Kumar, B. P. Singh, R. Prasad, and R. K. Bhowmik, Phys. Rev. C **85**, 034614 (2012); A. Yadav, V. R. Sharma, P. P. Singh, D. P. Singh, R. Kumar, Unnati, M. K. Sharma, B. P. Singh, R. Prasad, and R. K. Bhowmik, *ibid.* **85**, 064617 (2012).
[24] P. P. Singh *et al.*, Phys. Lett. B **671**, 20 (2009).
[25] J. Wilczyński, K. Siwek-Wilczyńska, J. van Driel, S. Gonggrijp, D. C. J. M. Hageman, R. V. F. Janssens, J. Łukasiak, and R. H. Siemssen, Phys. Rev. Lett. **45**, 606 (1980), and references therein.

[26] B. S. Tomar, A. Goswami, A. V. R. Reddy, S. K. Das, P. P. Burte, S. B. Manohar, and B. John, Phys. Rev. C **49**, 941 (1994); B. S. Tomar, A. Goswami, G. K. Gubbi, A. V. R. Reddy, S. B. Manohar, B. John, and S. K. Kataria, *ibid.* **58**, 3478 (1998).
[27] T. Inamura *et al.*, Phys. Lett. B **68**, 51 (1977); **84**, 71 (1979).
[28] C. Gerschel, Nucl. Phys. A **387**, 297 (1982).
[29] W. Trautmann, O. Hansen, H. Tricoire, W. Hering, R. Ritzka, and W. Trombik, Phys. Rev. Lett. **53**, 1630 (1984).
[30] I. Tserruya, V. Steiner, Z. Fraenkel, P. Jacobs, D. G. Kovar, W. Henning, M. F. Vineyard, and B. G. Glagola, Phys. Rev. Lett. **60**, 14 (1988).
[31] T. Udagawa and T. Tamura, Phys. Rev. Lett. **45**, 1311 (1980).
[32] J. P. Bondrof *et al.*, Nucl. Phys. A **333**, 285 (1980).
[33] H. P. Morsch, M. Rogge, P. Turek, and C. Mayer-Böricke, Phys. Rev. Lett. **45**, 337 (1980).
[34] R. Weiner *et al.*, Nucl. Phys. A **286**, 282 (1977).
[35] V. I. Zagrebaev, Ann. Phys. (NY) **197**, 33 (1990).
[36] B. G. Harvey, Nucl. Phys. A **444**, 498 (1985).
[37] M. H. Simbel and A. Y. Abdul Magd, Z. Phys. A **294**, 277 (1980).
[38] A. Y. Abdul Magd, Z. Phys. A **298**, 143 (1980).
[39] H. Mogenstern, W. Bohne, W. Galster, D. G. Kovar, and H. Lehr, Phys. Lett. B **113**, 463 (1982).
[40] H. Mogenstern, W. Bohne, W. Galster, and K. Grabisch, Z. Phys. A **324**, 443 (1986).
[41] FREEDOM, data acquisition and analysis system designed to support the accelerator based experiments at the Nuclear Science Centre, New Delhi, India.
[42] E. Browne and R. B. Firestone, *Table of Radioactive Isotopes* (Wiley, New York, 1986).
[43] O. B. Tarasov and D. Bazin, Nucl. Instrum. Methods Phys. Res., Sect. B **204**, 174 (2003).
[44] A. Gavron, Phys. Rev. C **21**, 230 (1980).
[45] R. Bass, Nucl. Phys. A **231**, 45 (1974).
[46] F. D. Becchetti and G. W. Greenlees, Phys. Rev. **182**, 1190 (1969).
[47] P. M. Endt, At. Data Nucl. Data Tables **26**, 47 (1981).
[48] S. K. Kataria, V. S. Ramamurthy, and S. S. Kapoor, Phys. Rev. C **18**, 549 (1978).
[49] J. P. Lestone, Phys. Rev. C **53**, 2014 (1996).
[50] J. Wilczynski *et al.*, Nucl. Phys. A **373**, 109 (1982).
[51] K. Siwek-Wilczyńska, E. H. du Marchievan Voorthuysen, J. van Popta, R. H. Siemssen, and J. Wilczyński, Phys. Rev. Lett. **42**, 1599 (1979).
[52] D. J. Parker, J. J. Hogan, and J. Asher, Phys. Rev. C **35**, 161 (1987); D. J. Parker, J. Asher, T. W. Conlon, and I. Naqib, *ibid.* **30**, 143 (1984).
[53] K. Hagino *et al.*, Comput. Phys. Commun. **123**, 143 (1999).
[54] R. Lindsay and N. Rowley, J. Phys. G **10**, 805 (1984).